Heating of microstructured optical fibers due to absorption of the propagating light

Alireza Hassani, Elio Pone, and Maksim Skorobogatiy

Department of Engineering Physics, École Polytechnique de Montréal, C.P. 6079, Succursale Centre-Ville, Montréal, Québec H3C 3A7, Canada

Received August 15, 2006; revised December 4, 2006; accepted December 5, 2006; posted December 7, 2006 (Doc. ID 74034); published March 15, 2007

Numerical and analytical models of the heat transfer in gas-filled microstructured optical fibers exhibiting material absorption of the propagating light are presented. The simulation domain is subdivided into two parts, with finite-difference discretization used in the microstructured region and analytical expansion used in the homogeneous cladding region. An intuitive analytical model is then developed to account for the fiber heating, demonstrating good agreement with the numerical method. In the application to the problem of temperature distribution in holey fibers, we find that maximal temperature rise in such fibers is a sensitive function of the diameter-to-pitch ratio while being only weakly sensitive to the wavelength-to-pitch ratio. © 2007 Optical Society of America

OCIS codes: 060.2280, 120.6810.

1. INTRODUCTION

An unprecedented flexibility in the design of transverse geometries makes microstructured optical fibers (MOFs) highly desirable for a multitude of applications in telecommunication, sensing, and high-power transmission. For a particular application, the cross section of MOFs can incorporate various arrangements of holes, layers, and irregular inclusions of various materials. These features can result in rich thermal and thermo-optic characteristics of MOFs compared with conventional fibers. Our paper studies the reduction of effective thermal conductivity and a consequent temperature increase in the gas-filled microstructured fibers. In such fibers, a porous MOF structure surrounding the fiber core serves as a thermal isolation layer, resulting in the increased fiber heating.

Recently, several devices using various aspects of MOF thermal response have been reported. Cladding-mode resonances in hybrid polymer–silica MOF gratings,[1] coherent resonances in periodic microfluidic MOF structures,[2] optical birefringence in hybrid MOFs,[3] and dispersion in photonic bandgap MOFs[4,5] can be efficiently tuned by temperature. Thermo-optic switching in liquid-crystal-infiltrated MOFs[6–8] and dependency of the Brillouin frequency shift on temperature in germanium-doped solid-core MOFs[9] have been reported. Birefringent solid-core MOFs can be designed to be either ultrasensitive or insensitive to temperature,[10–13] and thermally insensitive MOFs are used in interferometers to reduce the effect of temperature fluctuations.[14–16] The thermal phase sensitivity of the fundamental mode of an air-core MOF is found to be three to six times smaller than that of SMF28 fibers,[17] which could be beneficial for fiber-optic gyroscopes. Finally, transport of high-power laser pulses through the hollow-core or large-mode-area MOFs has been recently studied for applications in sensing, industrial, and medical applications.

We distinguish three broad categories of the heat transfer effects related to MOFs: (a) heat transfer during the fiber-drawing process[18–22]; (b) effect of the ambient temperature on the modal optical properties, assuming uniform temperature distribution in the fiber[17,23]; and (c) nonuniform heating in the fiber cross section caused by material absorption of the high-power light. Our study falls into a third category and is especially relevant for the understanding of the power capacity limitation of high-power-transmitting MOFs. Prior art in this area includes semianalytical analysis of heating in hollow-core Bragg fibers,[24] as well as finite-element analysis of heating of the MOF-based lasers.[25]

To our knowledge, no simple analytical model verified against a rigorous numerical method has so far been proposed to describe temperature rise in the air-core or solid-core MOFs due to material absorption of the propagating light. This study is also motivated by the recent advances in plastic MOF fabrication technology,[26–28] which opens up the possibility of relatively high-power transmission through plastic fibers for medical and sensing applications where the effects of heating could be substantial. In what follows we start with a rigorous numerical model for the heat transfer in MOFs and conclude by presenting a simple intuitive analytical model for the heat transfer in both solid- and hollow-core MOFs.

2. FORMULATION OF THE NUMERICAL METHOD

In this paper we consider a steady-state regime for the heat transfer in MOFs featuring an arrangement of gas-filled holes (Fig. 1). The governing equation for the heat conduction across the body of the fiber is given by

$$-k\nabla^2 T = Q, \tag{1}$$

where k, T, and Q denote the thermal conductivity, temperature, and heat source, respectively. A zero-flux bound-

 © 2007 Optical Society of America

ary condition is considered on the hole boundaries, as thermal conductivity of gases is negligible compared with that of a solid-fiber material:

$$-k\,\nabla T\cdot\mathbf{n}=0, \tag{2}$$

where $\mathbf{n}$ is the unit vector normal to the hole boundary. Moreover, radiation heat transfer across the gas-filled holes can be considered negligible compared with the heat flux through the solid vanes adjacent to the holes. In fact, it is easy to estimate the region of validity of this approximation. When we denote ΔT to be the temperature differential across one of the holes and T_f to be the average fiber temperature and assume that the effective thickness and length of the vane are $(\Lambda-d)$ and Λ, respectively, then the heat flux through the vane is $\sim k(\Lambda-d)\Delta T/\Lambda$, while the radiation flux in the hole is $\sim 4\pi\sigma d T_f^3\Delta T$. Finally, the linear approximation is valid when $4\pi\sigma d T_f^3/[k(1-d/\Lambda)]\ll 1$, which is well satisfied for all the examples in this paper, assuming room-temperature operation of the fibers.

Finally, we assume that the heat is transferred to the ambient through the circular outer fiber boundary by convection described by

$$-k\,\nabla T\cdot\mathbf{n}=h(T-T_{\mathrm{ambient}}), \tag{3}$$

where h is the heat transfer coefficient. The radiative heat transfer can again be considered negligible because of the insignificant temperature differences.[4]

The heat source is generated by the fiber material absorption of the propagating light. The source is concentrated in the region of overlap of the modal electromagnetic field and the region of high fiber material absorption. For complex fields, the heat source of a single-fiber mode normalized to P W of incoming power can be presented as[24]

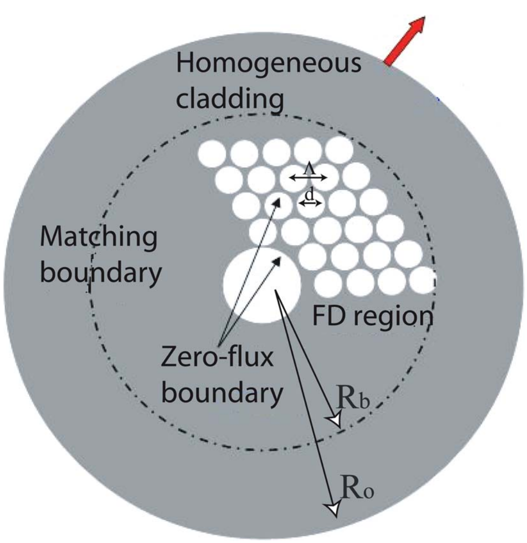

Fig. 1. (Color online) Schematic of a cross section of a gas-filled MOF showing finite-difference and analytical expansion regions and various boundary conditions.

$$Q=P\frac{2\pi\,\mathrm{Im}(\epsilon)}{\lambda}\frac{|\mathbf{E}|^2}{\mathrm{Re}\left[\int \mathrm{d}\mathbf{a}\cdot(\mathbf{H}^*\times\mathbf{E})\right]}, \tag{4}$$

where ϵ is the material dielectric constant, λ is the wavelength, and $\mathbf{E}$ and $\mathbf{H}$ are the electric and magnetic field vectors of the propagating mode. The power normalization integral in the denominator is extended over the fiber cross section. Electromagnetic field components can be calculated using any type of a vectorial mode solver. In this paper we use the multipole method[29] to obtain modal fields and to compute the heat source [Eq. (4)].

To solve the heat transfer equation (1), we use the finite-difference method in the microstructured region, which we then match at the intermediate circular interface with an analytical expansion in the uniform cladding region. Using analytical expansion in the large uniform fiber cladding considerably simplifies the solution of the complete heat transfer problem, allowing fine spatial discretization in a relatively small microstructured region.

The finite-difference method considered in this paper is based on the control volume approach.[30] In this method, the physical region is discretized into the nonoverlapping rectangular cells, and, within each cell, conservation of energy in the integral form is applied:

$$\int_C(\partial T/\partial n)\mathrm{d}C+\int_S(Q/k)\mathrm{d}S=0. \tag{5}$$

Here C and S stand for the boundary contour and cell area. For the cells inside the microstructured domain, Taylor series are used to approximate the integrals in Eq. (5) to the second order of accuracy in spatial discretization. For the cells on the boundary between the finite-difference and analytical domains, we first extend the discretization grid somewhat into the analytical domain and then again use Taylor series to approximate the integrals in Eq. (5) to the second order, while calculating the temperatures on the grid points in the analytical region using analytical expansion. Finally, for the cells located at the boundary of air holes, we use the boundary condition (2) together with Taylor series to arrive at a second-order accurate discretization of Eq. (5).

The choice of a contour where the matching between the finite-difference method and the analytical expansion is performed is somewhat arbitrary. In the case of a guided mode for which the modal fields are predominantly concentrated in the fiber core, the heat source will be also localized in the core. In what follows we always choose the boundary between the finite-difference and the analytical regions to be far enough from the core region so that the heat source in the analytical region can be considered negligible. For numerical convenience we assume this boundary to be a circle centered at the origin. The analytical region then presents a homogeneous cylindrical shell where, in the absence of a heat source, an exact analytical expansion[31] for the temperature distribution can be used:

$$T^{\mathrm{AN}} = c_1 + c_2 \log(r) + \sum_{m=-M,m\neq 0}^{M} A_m (R_b/r)^m \cos(m\theta) + \sum_{m=-M,m\neq 0}^{M} B_m (R_b/r)^m \sin(m\theta), \tag{6}$$

where r and θ are the cylindrical coordinates of the spatial points; R_b is the radius of the circular boundary between the numerical and the analytical regions; and c_1, c_2, A_m, and B_m are expansion coefficients to be determined by matching the finite-difference and analytical solutions at the boundary. The series are truncated at a finite M, which is chosen to be large enough to achieve convergence. Moreover, if symmetries are present, some of the coefficients in Eq. (6) will be 0. In what follows we study the MOF with C_{6v} symmetry. Intensity distributions of its modes exhibit two mirror symmetries with respect to the x and y axes (also implemented in a finite-difference computational scheme). Such symmetries cause all the sine terms and odd cosine terms to disappear from the summation [Eq. (6)].

Convection boundary conditions [Eq. (3)] can be easily incorporated into the analytical expansion. By substituting Eq. (6) into Eq. (3) one can eliminate some of the coefficients to find a modified analytical expansion satisfying both Eq. (3) and the above-mentioned symmetry considerations:

$$T^{\mathrm{AN}} = c_2[\log(r) + \alpha] + \sum_{m=\mathrm{even},m>0} \{A_m[(R_b/r)^m + \beta] + \tilde{A}_m[(r/R_b)^m + \gamma]\}\cos(m\theta), \tag{7}$$

where $\alpha=[-\log(R_o)-k/hR_o]$, $\beta=(mkR_b^m/hR_o^{m+1})-(R_b/R_o)^m$, $\gamma=-(mkR_o^{m-1}/hR_b^m)-(R_o/R_b)^m$, and R_o is the outer radius of the fiber.

We then enforce self-consistency of the finite-difference and analytical expansion descriptions on the boundary of the two domains by minimizing the objective function using the least-squares method:

$$\mathrm{LS} = \sum_i (T_i^{\mathrm{AN}} - T_i^{\mathrm{FD}})^2. \tag{8}$$

Here, T^{FD} is a temperature on a finite-difference discretization mesh, T^{AN} is a temperature given by the analytical expansion (7), and index i spans the finite-difference mesh points on the domain boundary.

Parameters c_2 and A_m, which minimize the objective function (8), can be found from a standard set of equations in the form

$$\partial\mathrm{LS}/\partial c_2 = 0 \Rightarrow \sum_i (T_i^{\mathrm{AN}} - T_i^{\mathrm{FD}})\log(r_i) = 0, \tag{9}$$

$$\partial\mathrm{LS}/\partial A_p = 0 \Rightarrow \sum_i (T_i^{\mathrm{AN}} - T_i^{\mathrm{FD}})[(R_b/r_i)^p + \beta]\cos(p\theta_i) = 0, \tag{10}$$

$$\partial\mathrm{LS}/\partial \tilde{A}_p = 0 \Rightarrow \sum_i (T_i^{\mathrm{AN}} - T_i^{\mathrm{FD}})[(r_i/R_b)^p + \gamma]\cos(p\theta_i) = 0, \tag{11}$$

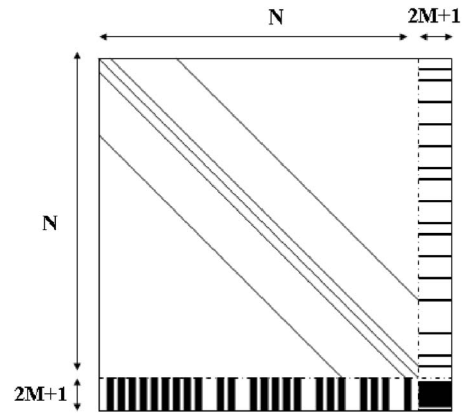

Fig. 2. Typical pattern of a sparse matrix corresponding to the heat transfer problem in microstructured fibers. First, N rows of a matrix result from N finite-difference flux conservation equations (5), and the last $2M+1$ matrix rows result from temperature-matching equations (12) on the boundary between the finite-difference and the analytical domains.

$$T_i^{\mathrm{AN}} - T_i^{\mathrm{FD}} = c_2[\log(r_i) + \alpha] + \sum_m A_m[(R_b/r_i)^m + \beta]\cos(m\theta_i) + \sum_m \tilde{A}_m[(r_i/R_b)^m + \gamma]\cos(m\theta_i) - T_i^{\mathrm{FD}}, \tag{12}$$

where $m=[2,4,\ldots,2M]$, and i spans the points on a finite difference grid at the boundary with an analytical region. We now define N as the number of finite-difference grid points.

Finally, to obtain temperature distribution over the fiber cross section, one has to solve simultaneously $N+2M+1$ linear equations (with an equal number of unknowns), where N equations result from the heat-flux conservation in each of the finite-difference cells [Eq. (5)] and the other $2M+1$ equations result from temperature matching [Eq. (12)] on the boundary between the finite-difference and analytical domains. In other words, a linear problem in the form $C\bar{x}=\bar{b}$ has to be solved with a $(N+2M+1)\times(N+2M+1)$ matrix C having the sparsity pattern of Fig. 2. We find that the biconjugate gradient method with incomplete LU preconditioning (ILU-BCG) works well for this type of problem. Thus, using the ILU-BCG we can routinely handle matrices of size $(300{,}000\times 300{,}000)$, and it takes several minutes to find a solution using a 2 GHz desktop personal computer. To handle even larger matrices, one can use a variant of a cyclic reduction algorithm adopted for boundary-value problems.[32] This allows us to work with sparse matrices of size up to $(700{,}000\times 700{,}000)$.

3. TEMPERATURE DISTRIBUTION IN MICROSTRUCTURED OPTICAL FIBERS

We use this developed method to analyze heat transfer in a solid-core MOF featuring three layers of hexagonally arranged holes (see inset of Fig. 3). We assume that the fiber is made of material with refractive index 1.5, which can be either silica or a polymer. For all the simulations presented in this paper, the MOF parameters are chosen as follows: microstructure pitch $\Lambda=2$ μm, outside fiber radius $R_o=125$ μm, convection heat transfer coefficient $h=25$ W/m^2 K, and thermal conductivity of the fiber material $k=0.25$ W/mK. After conducting detailed convergence studies, we choose numerical parameters to give relative errors in temperature smaller than 1%. These parameters are as follows: spatial discretization size $\Delta=25$ nm, position of a matching interface between the finite-difference and analytical domains $R_b=3.5\Lambda=7$ μm, and maximal angular momentum $M=4$.

In Fig. 3 we present temperature rise with respect to the ambient as a function of the hole diameter-to-pitch ratio for the fundamental mode of the MOF described above. Particularly, we compare the temperature in the center of the fiber core (maximal temperature) to the angle-averaged temperature on a circle of radius R_b located immediately outside the microstructured region. Wavelength of operation is $\lambda=1.55$ μm, and the heat source generated by the fundamental mode is concentrated in the fiber core. In the first example the fiber material is assumed to be glass with 0.2 dB/km material loss. When the hole diameter increases beyond 0.8Λ, the microstructured cladding becomes highly porous, hence less heat conductive, resulting in a considerable temperature difference between the fiber core and the uniform part of the cladding. In the inset of Fig. 3 we show the temperature distribution in the fiber cross section when the hole diameter is $d=0.8\Lambda$. Outside the microstructured region, temperature distribution can be well approximated as being angle independent. Note that when the hole diameter $d/\Lambda \ll 1$ is small, from the heat transfer point of view the microstructured region starts resembling a homogeneous cylindrical shell. In this regime, maximal temperature in the center of a MOF will be almost identical to the one in a conventional step-index fiber with otherwise comparable geometrical, material, and thermal parameters. For example, from Fig. 3 it follows that a silica MOF fiber with $d/\Lambda=0.98$ will exhibit 0.016 K/W temperature rise in the fiber center, while a silica step-index fiber of the same outside diameter will exhibit only 0.01 K/W temperature rise.

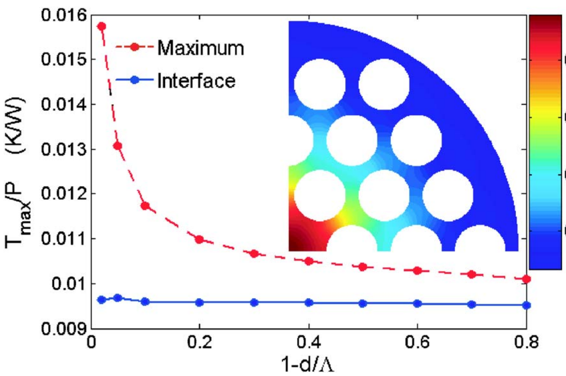

Fig. 3. (Color online) Temperature rise with respect to the ambient as a function of a hole diameter-to-pitch ratio for a fundamental mode of a MOF. Dotted curve, temperature at the fiber center; solid curve, temperature at the matching interface (right outside of the microstructure region). Fiber material is glass with 0.2 dB/km absorption loss, and 1 W of incoming power is assumed. From the figure we observe that microstructured cladding becomes a poor heat conductor for larger-size air holes.

As shown later, temperature rise in the uniform fiber cladding is largely determined by the value of a heat transfer coefficient h characterizing heat exchange efficiency through the fiber's outer boundary. On the other hand, the temperature difference between the fiber core and the uniform cladding is defined by the thermal conductivity k of a fiber material and geometry of a microstructure. In Fig. 4, the nondimensional temperature rise $[k\lambda\Delta T/\mathrm{Im}(\epsilon)P]$ across the microstructured region is presented as a function of $1-d/\Lambda$ for three different values of the normalized wavelength $\lambda/\Lambda=[0.1,0.5,1]$. Given a particular fiber geometry, the nondimensional temperature allows us to plot a single universal temperature curve for

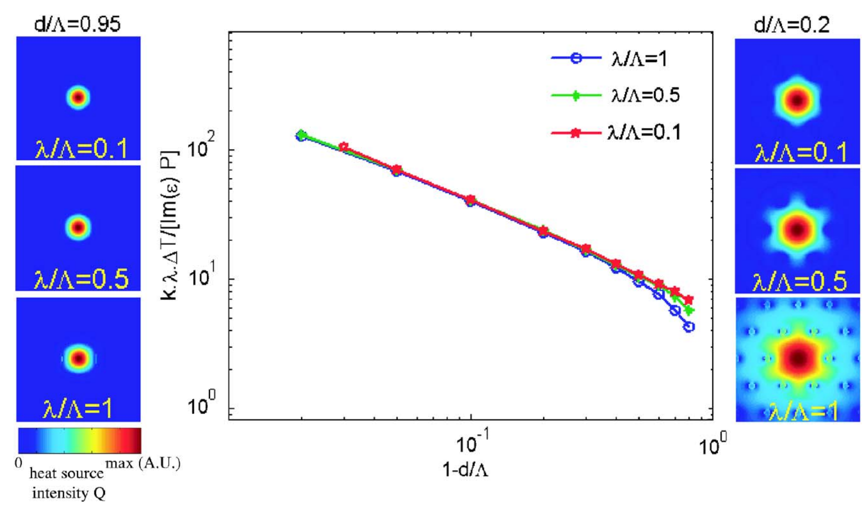

Fig. 4. (Color online) Temperature differential across the microstructured region as a function of $1-d/\Lambda$ for the three different values of normalized wavelength $\lambda/\Lambda=[0.1,0.5,1]$. Note that for the large hole diameters the temperature differential is almost independent of the normalized wavelength while becoming weakly sensitive to it for the small hole diameters $d/\Lambda<0.4$. Insets: heat source [Eq. (4)] distributions due to material absorption of a fundamental core mode for two different fibers and three different wavelengths.

any values of the material loss and thermal conductivity. Moreover, from Fig. 4 it is seen that for the larger hole diameters $d/\Lambda > 0.4$ the temperature is almost independent of the λ/Λ ratio. To explain this behavior, we study spatial distributions of heat sources (insets of Fig. 4) for the two extreme values of d/Λ and all three values of λ/Λ. From the insets we observe that, regardless of the wavelength, for the larger d/Λ ratios the heat source is completely concentrated in the fiber core, thus leading to similar thermal distributions. For smaller d/Λ, the modal field and a corresponding heat source become delocalized in the microstructured region with a degree of delocalization sensitive to the wavelength of operation. This modal behavior results in a complex, wavelength-dependent temperature distribution.

To summarize, from Fig. 4 we conclude that for large hole diameters $d/\Lambda > 0.4$ the temperature rise across the microstructured cladding is a universal function independent of the wavelength of light with $k\lambda\Delta T/\mathrm{Im}(\varepsilon)P \sim 1/(1-d/\Lambda)^{0.8}$.

4. ANALYTICAL MODEL FOR THE ANGLE-AVERAGED TEMPERATURE DISTRIBUTION

We now present a simple analytical model for the angle-averaged temperature distribution across the MOF cross section, assuming that all the heat is generated in the core region. In such a model each layer of holes is approximated as a uniform cylinder with its own effective heat resistivity. The temperature differential across a set of concentric cylinders is then written as[33] $\Delta T = qZ_{\mathrm{tot}}$, where q is the total radial heat flux per unit of fiber length and Z_{tot} is the total heat resistance of a set of cylinders. The heat resistance of a fiber cross section is then $Z_{\mathrm{tot}} = Z_{\mathrm{core}} + Z_{\mathrm{micr}} + Z_{\mathrm{unif}} + Z_{\mathrm{conv}}$, where Z_{core}, Z_{micr}, Z_{unif}, and Z_{conv} are the heat resistance of the core, microstructured part of the cladding, uniform part of the cladding, and outer boundary of the fiber with convection boundary conditions, respectively.

In our model, the fiber core is considered a homogeneous cylinder with radius R_c with a uniformly distributed heat source generating total radial flux q leaving the core. According to Ref. 33, heat resistance of the core is given by $Z_{\mathrm{core}} = 1/4\pi k$, where k is the thermal conductivity of the fiber material. The uniform cladding is a cylindrical shell with heat resistance given by $Z_{\mathrm{unif}} = \ln(R_o/R_b)/2\pi k$, where, as before, R_o is the fiber outer radius and R_b is the outer radius of the microstructured region. Heat resistance of the outer fiber interface with the convection boundary condition is $Z_{\mathrm{conv}} = 1/2\pi h R_o$ where h is the heat transfer (convection) coefficient. In what follows, we find an analytical approximation for the resistivity of microstructured cladding Z_{micr}.

Sixfold symmetry allows us to consider only one sixth of the fiber cross section. In Fig. 5 we present an approximation to the elementary heat flows in the microstructured part of the fiber. Arrows represent heat-flow paths in the different layers of holes. We define heat resistivity of a single segment connecting the two closest points on a honeycomb lattice as Z_{seg}. Net heat flow across the first layer involves only six segments. In the second layer there are $6(2+2)$ segments, in the third one there are $6(4+3)$ segments, while in the Nth layer there are $6[2(N-1)+N]$ segments. Correspondingly, the heat resistance of the first, second, third, and the Nth layers are $Z_{\mathrm{seg}}/6$, $(Z_{\mathrm{seg}}/2+Z_{\mathrm{seg}}/2)/6$, $(Z_{\mathrm{seg}}/4+Z_{\mathrm{seg}}/3)/6$, and $[Z_{\mathrm{seg}}/2(N-1)+Z_{\mathrm{seg}}/N]/6$, respectively. Finally, one obtains the net heat resistance of a microstructured cladding by summing over all the N_l layers:

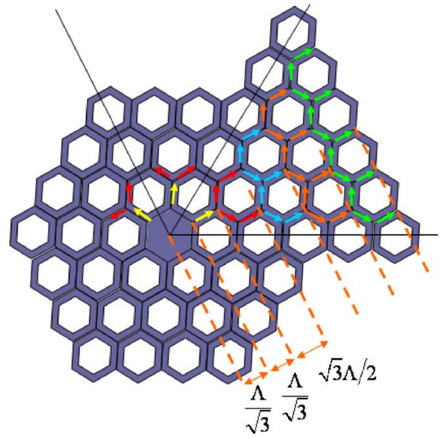

Fig. 5. (Color online) Approximation to the heat flow in the microstructured part of the fiber cladding.

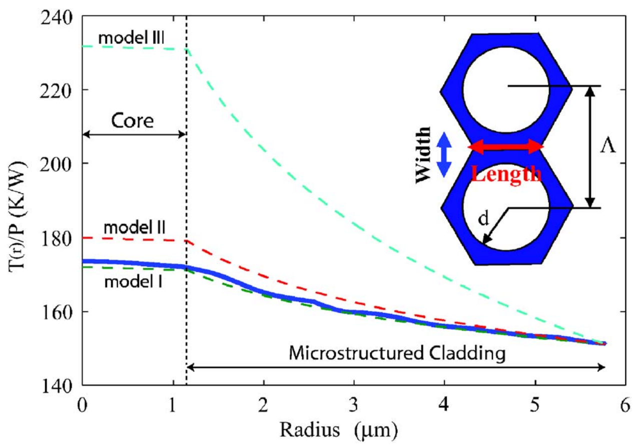

Fig. 6. (Color online) Angle-averaged temperature rise with respect to the ambient in a three-layer holey fiber. Solid curve, finite-difference method; dashed curves, three analytical models corresponding to the different approximations [Eqs. (14)–(16)] of the effective thermal conductivity of microstructured cladding.

$$Z_{\mathrm{mirc}} = \frac{Z_{\mathrm{seg}}}{6}\left\{1 + \sum_{n=2}^{N_l}\left[\frac{1}{2(n-1)} + \frac{1}{n}\right]\right\} \simeq \frac{Z_{\mathrm{seq}}}{4}\ln(N_l). \tag{13}$$

Several models for the segment resistivity Z_{seg} can be readily derived by approximating a material vane between the two holes (inset of Fig. 6) as a rectangular rod of some effective length L and width W with $Z_{\mathrm{seg}} = L/k\mathrm{W}$. In all the models the length of the segment is assumed to be $L = \Lambda/\sqrt{3}$. In model I the effective width is found directly from the area conservation as $6(W/2)L = (A_{\mathrm{hexagone}} - A_{\mathrm{circle}})$, leading to

$$\text{model I:}Z_{\text{seg}} = 1 \Bigg/ \left\{ k\left[\frac{\sqrt{3}}{2} - \frac{\pi}{4}\left(\frac{d}{\Lambda}\right)^2\right]\right\}. \quad (14)$$

The disadvantage of model I is that in the limit of $d \to \Lambda$ it does not reproduce physically intuitive infinite resistivity. To correct for this shortcoming in model II, we assume the holes to be hexagonally shaped with the edge-to-edge distance d (see Fig. 5). From the area conservation argument we then get

$$\text{model II:}Z_{\text{seg}} = 1 \Bigg/ \left\{ k\frac{\sqrt{3}}{2}\left[1 - \left(\frac{d}{\Lambda}\right)^2\right]\right\}, \quad (15)$$

with resistivity going to infinity for $d \to \Lambda$. Finally, in model III we simply assume that $W = \Lambda - d$, leading to

$$\text{model III:Z}_{\text{seg}} = 1 \Bigg/ \left[k\sqrt{3}\left(1 - \frac{d}{\Lambda}\right)\right], \quad (16)$$

which is the least precise of the three models as the area conservation argument is not used in the derivation.

We now derive effective thermal conductivity of a microstructured cladding. Comparing the expression for the heat resistance of a microstructured region [expression (13)] with that of a homogeneous shell $Z_{\text{micr}} = \ln(R_b/R_c)/2\pi k_{\text{micr}}$ of effective thermal conductivity k_{micr} with internal and external radii $R_c = \Lambda/\sqrt{3}$, $R_b = \Lambda[(N_l - 1)\sqrt{3}/2 + 2/\sqrt{3}]$, we find

$$k_{\text{micr}} \simeq 2/(\pi Z_{\text{seg}}), \quad (17)$$

which becomes almost an equality for $N_l > 2$. From expression (17) we conclude that effective thermal conductivity of a microstructured region reduces considerably when the hole diameter approaches the pitch, thus leading to thermal isolation of the fiber core from the uniform cladding.

Finally, we present an analytical model that describes the effect of thermal isolation of the fiber core by microstructured cladding and compare its predictions with those of the finite-difference method. We start by calculating the total heat flux per unit fiber length q leaving the fiber core into the microstructured cladding. From energy conservation, total heat flux is equal to the absorbed optical power in the core $q = P\alpha$, where P (watts) is the power in the propagating mode, while α (inverse meters) is the modal absorption loss coefficient. If the fiber is truly guiding (no radiation loss), then the modal absorption loss coefficient is defined by the imaginary part of the modal effective refractive index $\alpha = \text{Im}(n_{\text{eff}})4\pi/\lambda$. However, when both radiation and absorption losses are present, as is the case in a MOF with a finite microstructured cladding, the heat flux is generated only via absorption, and the two mechanisms have to be distinguished. To obtain the correct expression for the heat flux, we first use the mode solver on a fiber with a strictly real dielectric profile $\text{Re}(\epsilon)$ to obtain modal radiation losses $\sim \text{Im}(n_{\text{eff}}^{\text{rad}})$. Then the mode solver is used a second time on a fiber with a complex dielectric profile ϵ describing material absorption to obtain total modal transmission loss $\sim \text{Im}(n_{\text{eff}}^{\text{rad+abs}})$. Finally, total heat flux generated via material absorption of a propagated light is calculated as

$$q = P\,\text{Im}(n_{\text{eff}}^{\text{rad+abs}} - n_{\text{eff}}^{\text{rad}})4\pi/\lambda. \quad (18)$$

Alternatively, perturbation theory expressions can be used to evaluate modal loss due to absorption.[34] As a reference, the imaginary part of the refractive index of a bulk material featuring absorption loss γ (decibels per meter) is $\text{Im}(n_{\text{bulk}}) = \gamma\lambda \ln(10)/(40\pi)$, where λ is the wavelength.

Final expressions for the analytical model of the angle-averaged temperature distribution in a microstructured fiber cross section are

$$T(r) = q\left[\frac{\ln(R_o/r)}{2\pi k} + \frac{1}{2\pi h R_o}\right], \qquad R_b \leqslant r \leqslant R_o,$$

$$T(r) = q\left[\frac{\ln(R_b/r)}{2\pi k_{\text{micr}}} + \frac{\ln(R_o/R_b)}{2\pi k} + \frac{1}{2\pi h R_o}\right],$$
$$R_c \leqslant r \leqslant R_b,$$

$$T(r) = q\left[\frac{1}{4\pi k}\left(1 - \frac{r^2}{R_c^2}\right) + \frac{\ln(R_b/R_c)}{2\pi k_{\text{micr}}} + \frac{\ln(R_o/R_b)}{2\pi k} + \frac{1}{2\pi h R_o}\right], \qquad 0 \leqslant r \leqslant R_c, \quad (19)$$

where effective heat conductivity is defined by expression (17) and total heat flux is defined by Eq. (18).

In Fig. 6 we present a comparison of the analytical model [Eqs. (19)] with the angle-averaged temperature distribution computed by the finite-difference method. We consider again a hexagonal solid-core MOF with three layers of holes and $d/\Lambda = 0.9$, $\Lambda = 2\ \mu\text{m}$, $\lambda = 1.55\ \mu\text{m}$. The fiber material is assumed to have a bulk absorption loss $\gamma = 3\ \text{dB/m}$ corresponding to that of low-optical-quality polymers. Temperature rise is computed for 1 W of incoming power. The thick solid curve in Fig. 6 corresponds to the angle-averaged finite-difference method, while dotted curves correspond to the three different analytical models. Both analytical models I and II show excellent agreement with finite-difference calculations, whereas model III results only in a qualitative agreement.

5. CONCLUSION

An efficient hybrid finite-difference method with analytical expansion in the cladding is developed to study heating of a microstructured fiber via material absorption of the propagating electromagnetic mode. The cladding of a MOF is divided into two regions—the microstructured region where the finite-difference discretization is used and the homogeneous cladding where the analytical expansion is exploited. Temperature on the boundary of the analytical and numerical domains is then matched by the least-squares method. It is found that, for a microstructured holey fiber with a hexagonal arrangement of large holes ($d/\Lambda > 0.4$), temperature rise in the fiber core shows a weak dependency on the wavelength of light-to-pitch ratio. Moreover, in this case, temperature differential across the microstructured cladding is found to be described by a universal curve $k\lambda\Delta T/\text{Im}(\epsilon)P \sim 1/(1 - d/\Lambda)^p$, $p \sim 0.8$. Finally, a simple, yet precise analytical model for the effective thermal conductivity coefficient of the microstructured cladding is developed.

M. Skorobogatiy, the corresponding author, can be reached by e-mail at maksim.skorobogatiy@polymtl.ca.

REFERENCES

1. P. S. Westbrook, B. J. Eggleton, R. S. Windeler, A. Hale, T. A. Strasser, and G. L. Burdge, "Cladding-mode resonances in hybrid polymer–silica microstructured optical fiber gratings," IEEE Photon. Technol. Lett. **12**, 495–497 (2000).
2. C. Kerbage, J. Ging, A. Hale, and B. J. Eggieton, "Coherent microfluidic resonance in microstructured optical fiber," in *The 15th Annual Meeting of the IEEE Lasers and Electro-Optics Society* (IEEE, 2002), Vol. 2, pp. 813–814.
3. C. Kerbage, P. Steinvurzel, A. Hale, R. S. Windeler, and B. J. Eggleton, "Birefringent tunable hybrid microstructured optical fiber," in *Conference on Lasers and Electro-Optics (CLEO)*, Vol. 73 of OSA Trends in Optics and Photonics Series (Optical Society of America, 2002), Vol. 1, p. 14.
4. R. T. Bise, J. Jasapara, P. Steinvurzel, and D. J. DiGiovanni, "Temperature tuning of dispersion in a photonic band gap fiber," in *Conference on Lasers and Electro-Optics (CLEO)*, Vol. 73 of OSA Trends in Optics and Photonics Series (Optical Society of America, 2002), pp. 614–615.
5. Y. Jiang, X. Chen, and B. Howley, "Effect of temperature fluctuation on highly dispersive photonic crystal fiber," Appl. Phys. Lett. **88**, 011108 (2006).
6. T. T. Larsen, J. Broeng, D. S. Hermann, and A. Bjarklev, "Thermo-optic switching in liquid crystal infiltrated photonic bandgap fibers," Electron. Lett. **39**, 1719–1720 (2003).
7. J. Lgsgaard and T. T. Alkeskjold, "Designing a photonic bandgap fiber for thermo-optic switching," J. Opt. Soc. Am. B **23**, 951–956 (2006).
8. T. R. Wolinski, K. Szaniawska, S. Ertman, P. Lesiak, A. W. Domanski, R. Dabrowski, E. Nowinowski-Kruszelnicki, and J. Wojcik, "Influence of temperature and electrical fields on propagation properties of photonic liquid-crystal fibers," Meas. Sci. Technol. **17**, 985–991 (2006).
9. L. Zou, X. Bao, Sh. Afshar, and L. Chen, "Dependence of the Brillouin frequency shift on strain and temperature in a photonic crystal fiber," Opt. Lett. **29**, 1485–1487 (2004).
10. A. Ortigosa-Blanch, A. Diez, M. Delgado-Pinar, J. L. Cruz, and M. V. Andres, "Temperature independence of birefringence and group velocity dispersion in photonic crystal fibers," Electron. Lett. **40**, 1327–1329 (2004).
11. T. Nasilowski, T. Martynkien, G. Statkiewicz, M. Szpulak, J. Olszewski, G. Golojuch, W. Urbanczyk, J. Wojcik, P. Mergo, M. Makara, F. Berghmans, and H. Thienpont, "Temperature and pressure sensitivities of the highly birefringent photonic crystal fiber with core asymmetry," Appl. Phys. B **81**, 325–331 (2005).
12. W. J. Bock and W. Urbanczyk, "Measurement of sensitivity of birefringent holey fiber to temperature, elongation, and hydrostatic pressure," in *Proceedings of the IEEE Instrumentation and Measurement Technology Conference* (IEEE, 2005), pp. 1228–1232.
13. M. Wegmuller, M. Legre, N. Gisin, T. Ritari, H. Ludvigsen, J. R. Folkenberg, and K. P. Hansen, "Experimental investigation of wavelength and temperature dependence of phase and group birefringence in photonic crystal fibers," in *Proceedings of Sixth International Conference on Transparent Optical Networks* (IEEE, 2004), pp. 111–114.
14. D. H. Kim and J. U. Kang, "Sagnac loop interferometer based on polarization maintaining photonic crystal fiber with reduced temperature sensitivity," Opt. Express **12**, 4490–4498 (2004).
15. C. L. Zhao, X. Yang, C. Lu, W. Jin, and M. S. Demokan, "Temperature-insensitive interferometer using a highly birefringent photonic crystal fiber loop mirror," IEEE Photon. Technol. Lett. **16**, 2535–2537 (2004).
16. J. Ju, Z. Wang, W. Jin, and M. S. Demokan, "Temperature sensitivity of a two-mode photonic crystal fiber interferometer," in *The 18th Annual Meeting of the IEEE Lasers and Electro-Optics Society* (IEEE, 2005), pp. 873–874.
17. V. Dangui, H. Kyun Kim, M. J. F. Digonnet, and G. S. Kino, "Phase sensitivity to temperature of the fundamental mode in air-guiding photonic bandgap fibers," Opt. Express **13**, 6669–6675 (2005).
18. K. Lyytikainen, J. Zagari, G. Barton, and J. Canning, "Heat transfer within a microstructured polymer optical fiber preform," Modell. Simul. Mater. Sci. Eng. **12**, S225–S265 (2004).
19. S. C. Xue, R. I. Tanner, G. W. Barton, R. Lwin, M. C. J. Large, and L. Poladian, "Fabrication of microstructured optical fibers—Part I: Problem formulation and numerical modeling of transient draw process," J. Lightwave Technol. **23**, 2245–2254 (2005).
20. S. C. Xue, R. I. Tanner, G. W. Barton, R. Lwin, M. C. J. Large, and L. Poladian, "Fabrication of microstructured optical fibers—Part II: Numerical modeling of steady-state draw process," J. Lightwave Technol. **23**, 2255–2266 (2005).
21. S. C. Xue, M. C. J. Large, G. W. Barton, R. I. Tanner, L. Poladian, and R. Lwin, "Role of material properties and drawing conditions in the fabrication of microstructured optical fibers," J. Lightwave Technol. **24**, 853–860 (2006).
22. E. Pone, C. Dubois, N. Gu, Y. Gao, A. Dupuis, F. Boismenu, S. Lacroix, and M. Skorobogatiy, "Drawing of the hollow all-polymer Bragg fibers," Opt. Express **14**, 5838–5852 (2006).
23. T. Martynkien, M. Szpulak, and W. Urbanczyk, "Modeling and measurement of temperature sensitivity in birefringent photonic crystal holey fibers," Appl. Opt. **44**, 7780–7788 (2005).
24. M. Skorobogatiy, S. A. Jacobs, S. G. Johnson, C. Anastassiou, and B. Temelkuran, "Heating of hollow photonic Bragg fibers from field propagation, coupling, and bending," J. Lightwave Technol. **23**, 3517–3525 (2005).
25. J. Limpert, T. Schreiber, A. Liem, S. Nolte, and H. Zellmer, "Thermo-optical properties of air-clad photonic crystal fiber lasers in high power operations," Opt. Express **11**, 2982–2990 (2003).
26. A. Argyros, M. A. van Eijkelenborg, M. C. J. Large, and I. M. Bassett, "Hollow-core microstructured polymer optical fiber," Opt. Lett. **31**, 172–174 (2006).
27. A. Dupuis, Y. Gao, N. Guo, E. Pone, N. Godbout, S. Lacroix, C. Dubois, and M. Skorobogatiy, "Biodegradable, double-core, porous optical fiber," in *Conference on Lasers and Electro-Optics (CLEO)*, OSA Trends in Optics and Photonics Series (Optical Society of America, 2006), postdeadline paper CPDB5.
28. A. Dupuis, N. Guo, Y. Gao, N. Godbout, S. Lacroix, C. Dubois, and M. Skorobogatiy, "Prospective for the biodegradable microstructured optical fibers," Opt. Lett. **32**, 109–111 (2007).
29. T. P. White, B. T. Kuhlmey, R. C. McPhedran, D. Maystre, G. C. M. de Sterke, and L. C. Botten, "Multipole method for microstructured optical fibers. I. Formulation," J. Opt. Soc. Am. B **19**, 2322–2330 (2002).
30. Y. Jaluria and K. E. Torrance, *Computational Heat Transfer* (Taylor & Francis, 2003).
31. M. N. Ozisik, *Heat Conduction*, 2nd ed. (Wiley, 1993).
32. P. Amodio and M. Paprzycki, "A cyclic reduction approach to the numerical solution of boundary value ODEs," SIAM J. Sci. Comput. (USA) **18**, 56–59 (1997).
33. J. P. Holman, *Heat Transfer*, 5th ed. (McGraw-Hill, 1981), pp. 32–34.
34. R. Guobin, W. Zhi, L. Shuqin, L. Yan, and J. Shuisheng, "Full-vectorial analysis of complex refractive-index photonic crystal fibers," Opt. Express **12**, 1126–1135 (2004).